Clinical Cancer Research

Evolutionary Routes in Metastatic Uveal Melanomas Depend on *MBD4* Alterations

Manuel Rodrigues[1,2], Lenha Mobuchon[1], Alexandre Houy[1], Samar Alsafadi[1,3], Sylvain Baulande[4], Odette Mariani[5], Benjamin Marande[3], Khadija Ait Rais[6], Monique K. Van der Kooij[7], Ellen Kapiteijn[7], Sieta Gassama[1], Sophie Gardrat[8], Raymond L. Barnhill[8,9], Vincent Servois[10], Rémi Dendale[11], Marc Putterman[12], Sarah Tick[13], Sophie Piperno-Neumann[2], Nathalie Cassoux[9,14], Gaëlle Pierron[6], Joshua J. Waterfall[1,3], Sergio Roman-Roman[3], Pascale Mariani[15], and Marc-Henri Stern[1,16]

Abstract

Purpose: Uveal melanomas (UM) are genetically simple tumors carrying few copy number alterations (CNA) and a low mutation burden, except in rare *MBD4*-deficient, hypermutated cases. The genomics of uveal melanoma metastatic progression has not been described. We assessed the genetic heterogeneity of primary and metastatic *MBD4*-proficient and -deficient uveal melanomas.

Experimental Design: We prospectively collected 75 metastatic and 16 primary samples from 25 consecutive uveal melanoma patients, and performed whole-exome sequencing.

Results: *MBD4*-proficient uveal melanomas contained stable genomes at the nucleotide level, acquiring few new single nucleotide variants (SNVs; 16 vs. 13 in metastases and primary tumors, respectively), and no new driver mutation. Five CNAs were recurrently acquired in metastases (losses of 1p, 6q, gains of 1q, 8q, and isodisomy 3). In contrast, *MBD4*-deficient uveal melanomas carried more than 266 SNVs per sample, with high genetic heterogeneity and *TP53*, *SMARCA4*, and *GNAS* new driver mutations. SNVs in *MBD4*-deficient contexts were exploited to unveil the timeline of oncogenic events, revealing that metastatic clones arose early after tumor onset. Surprisingly, metastases were not enriched in monosomy 3, a previously defined metastatic risk genomic feature. Monosomy 3 was associated with shorter metastatic-free interval compared with disomy 3 rather than higher rate of relapse.

Conclusions: *MBD4*-proficient uveal melanomas are stable at the nucleotide level, without new actionable alterations when metastatic. In contrast, *MBD4* deficiency is associated with high genetic heterogeneity and acquisition of new driver mutations. Monosomy 3 is associated with time to relapse rather than rate of relapse, thus opening avenues for a new genetic prognostic classification of uveal melanomas.

Introduction

Uveal melanoma is the most common ocular primary tumor representing approximately 5% of all melanomas (1). Uveal melanoma is, from a genetic point of view, one of the simplest adult tumors with few copy number variations, a remarkably low mutation burden and an absence of ultraviolet-related DNA damage (2). In the current paradigm, malignant transformation is thought to be due to two main early genetic events, of which the respective timing of occurrence is unknown (3). The first event, which leads to constitutive activation of the $G_{\alpha q}$ pathway, consists of activating hotspot mutations of either *GNAQ*/*GNA11* (encoding $G_{\alpha q}$ proteins), *CYSTLR2* (a $G_{\alpha q}$-coupled coupled receptor), or *PLCB4* (the isoform 4 of phospholipase C-β) genes (4–7). The second event consists of almost mutually exclusive alterations including either (i) the biallelic inactivation of *BAP1* (3p21), encoding a deubiquitinase involved in chromatin remodeling, frequently through chromosome 3 loss of heterozygosity and *BAP1* mutation; (ii) change-of-function heterozygous mutations of *SF3B1* or other genes encoding members of the splicing

[1]Institut Curie, PSL Research University, INSERM U830, Paris, France. [2]Institut Curie, PSL Research University, Department of Medical Oncology, Paris, France. [3]Institut Curie, PSL Research University, Translational Research Department, Paris, France. [4]Institut Curie, PSL Research University, Institut Curie Genomics of Excellence (ICGex) Platform, Paris, France. [5]Institut Curie, PSL Research University, Biological Resource Center, Paris France. [6]Somatic Genetic Unit, Department of Genetics, Institut Curie, PSL Research University, Paris, France. [7]Leiden University Medical Center, Leiden, the Netherlands. [8]Department of Biopathology, Institut Curie, PSL Research University, Paris, France. [9]Faculty of Medicine, University of Paris Descartes, Paris, France. [10]Department of Medical Imaging, Institut Curie, PSL Research University, Paris, France. [11]Department of Radiation Oncology, Institut Curie, PSL Research University, Paris, France. [12]Department of Pathology, Quinze-Vingts National Ophthalmology Hospital, Paris, France. [13]Department of Ophthalmology IV, Quinze-Vingts National Ophthalmology Hospital, Paris, France. [14]Department of Ocular Oncology, Institut Curie, PSL Research University, Paris, France. [15]Department of Surgical Oncology, Institut Curie, PSL Research University, Institut Curie, Paris, France. [16]Department of Genetics, Institut Curie, PSL Research University, Paris, France.

Note: Supplementary data for this article are available at Clinical Cancer Research Online (http://clincancerres.aacrjournals.org/).

M. Rodrigues and L. Mobuchon contributed equally to this article.

Corresponding Author: Marc-Henri Stern, INSERM U830, Institut Curie, 26 rue d'Ulm, Paris 75248, France. Phone: 331-56-24-6646; Fax: 331-53-10-40-41; E-mail: marc-henri.stern@curie.fr

Clin Cancer Res 2019;25:5513–24

doi: 10.1158/1078-0432.CCR-19-1215

Translational Relevance

Uveal melanoma is the most common eye tumor in Western countries and is associated with up to 50% of chemoresistant, metastatic recurrence. By comparing the genetic profiles of uveal melanoma metastases with paired primary tumors, we observed that uveal melanoma is a striking example of stability at the nucleotide level during the metastatic process, while acquiring few recurrent copy number alterations. The absence of new oncogenic drivers in uveal melanoma metastases allows clinicians to dispense with biopsy of metastatic sites to search for drug targets. Conversely, two patients presented with hypermutated, highly heterogeneous, *MBD4*-deficient tumors. We took advantage of this phenotype and used it as a high-resolution genetic clock to deduce the tumors histories. Unexpectedly, we show that metastatic clones may arise very early during uveal melanoma tumorigenesis, long before diagnosis of the primary tumor, thus underscoring the need for new adjuvant strategies for this disease.

machinery; and (iii) hypomorphic mutations of *EIF1AX*, encoding a translation initiation factor (2, 3, 8–11). Another rare but recurrent genetic event in uveal melanoma is the inactivation of *MBD4*. *MBD4* encodes a glycosylase responsible for the repair of spontaneous deamination of methyl cytosine. Consistent with this activity, inactivation of *MBD4* is associated with a CpG>TpG hypermutation phenotype (12).

Uveal melanomas are diploid tumors with specific, recurrent copy number alterations (CNA) of whole chromosomes or arms including losses of 1p, 6q, 8p and gains of 1q, 6p, and 8q (13, 14). Monosomy 3 is one of the most frequent chromosomal imbalances in uveal melanoma and is frequently associated with *BAP1* mutation, while disomic 3 tumors are *SF3B1*- or *EIF1AX*-mutated, thus defining two types of uveal melanomas with different outcomes. Tumor size, gene expression profile, *BAP1* mutation, monosomy 3, gain of 8q (either the subtelomeric region, the whole arm or the whole chromosome), and 6p gain strongly predict the metastatic risk (8, 13–15). Despite successful treatment of the primary tumor, up to 50% of patients will eventually develop visceral metastases, mostly in the liver, with a poor median survival of less than 1 year (1, 16). To date, no chemotherapy or targeted therapy has improved the overall survival of metastatic patients (17). Even though a survival benefit has not been demonstrated in a controlled trial, complete, margin-free resection of metastases is often proposed when feasible (18).

Next-generation sequencing has widely expanded our knowledge of cancer genetics, but the overwhelming majority of studies have explored primary tumor collections with only few large series of metastatic tumors (19, 20). Remarkably, tumors such as skin melanomas, renal or pancreatic carcinomas have shown substantial genetic heterogeneity within tumors and during the metastatic process, which may be a key factor of drug resistance (21). Although genetic features of primary uveal melanoma have been well explored, the genetics and heterogeneity of uveal melanoma metastases remain largely uncharacterized (22, 23). This study aims to explore the intrapatient genetic heterogeneity of uveal melanoma during metastatic progression as a possible mechanism of chemoresistance, and to evaluate the influence of intrinsic and extrinsic mutational processes on tumor heterogeneity.

Materials and Methods

Sample collection

This study was conducted in accordance with the declaration of Helsinki and was approved by the Internal Review Board of Institut Curie (Paris, France). Patients eligible for margin-free resection (R0 resection) of suspected uveal melanoma liver metastases provided written informed consent to perform germline and somatic genetic analyses of resected metastases and archived frozen primary tumors. Germline DNA was extracted from unaffected tissue (liver in all cases but two, which were extracted from blood). Tumors were sampled within 10 minutes after resection. If sufficient material was available, every tumor was sampled at least once and largest ones were sampled several times in different regions, avoiding hemorrhagic and necrotic areas. Diagnosis of metastatic uveal melanoma was confirmed by a specialized pathologist. Mutation burdens and signatures of 24 cases from this series were reported previously (12).

Library preparation and sequencing

Samples were histologically reviewed by a pathologist before nucleic acids extraction to select samples with at least 30% of tumor cells. DNA were extracted using Phenol (Invitrogen), by the *Centre de Ressources Biologiques* (Institut Curie tumor biobank) and subsequently purified on Zymo-Spin IC (Zymo Research). DNAs were quantified by Qubit (Thermo Fisher Scientific). Whole-exome Sequencing (WES) libraries were prepared using the Agilent SureSelect XT2 Clinical Research Exome kit (Agilent Technologies) from 1 μg of DNA, isolated from initial libraries with median insert size of 300 bp according to the manufacturers' protocols. Libraries from primary tumors from cases #1 and #5 were prepared using the Agilent SureSelectXT HS kit (Agilent Technologies) with 20 ng of DNA-isolated initial libraries. The sample from case #1 and sample 1 from case #5 were obtained from enucleated eyes (500 ng from formalin-fixed paraffin-embedded tissue); sample 2 from case #5 was obtained from a frozen biopsy obtained before enucleation (15 ng). Libraries were 100-bp paired-end multiplex sequenced on the Illumina HiSeq 2500 (Illumina). WES depth was set *a priori* to sequence germline DNA at 30× and somatic DNA at 100×. Sequencing quality was assessed by FastQC. Reads were aligned to the human genome (hg19) with Bowtie2 2.1.0 (24). PCR duplicates were removed using Picard Tool MarkDuplicates v1.97.

Mutation calling

After removing duplicates, WES data underwent variant calling for SNVs and indels using the combination of three variant callers: HaplotypeCaller, MuTect2, and SAMtools mpileup (25–27). Union of variants detected with these three algorithms were annotated using ANNOVAR (28), with the following databases: ensGene, avsnp147 (29), cosmic80 (30), popfreq_all and dbnsfp33a. Somatic variants with less than 10 reads of DP in germline and/or less than 10 reads of somatic DP and/or at least 5 reads of germline AD and/or at least 10% of germline variant allele frequency (VAF) and/or less than 5 reads of somatic AD and/or a population frequency higher than 1% (popfreq_all>0.01) were filtered out. Finally, all somatic mutations called by this procedure were controlled manually using the Integrative Genomics Viewer (IGV) by at least two authors. Because alterations of *BAP1*, *EIF1AX*, and *SRSF2* in uveal melanoma may be difficult to call, these genes were entirely checked on IGV in all samples. After this first round, we aggregated the SNVs from all samples of one

case and search for these SNVs in all samples of this patient to recover true SNVs that may present at very low depth because of subclonality. The amount of mutations was compared with the different TCGA cohorts using the "maftools" R package version 1.6.15. Subclones in samples were determined with Pyclone version 0.13.0 (31). Cancer cell fraction (CCF) was also determined with Pyclone. SNVs were defined as "private" if present at more than 5% of corrected VAF ($0.5^{*}VAF_{SNV}/VAF_{GNAQ/GNA11}$) in one sample and less than 5% in the others.

Copy number alterations

Copy number gains and losses were determined from WES using Facets in R with default settings (32). Briefly, Facets provides copy number and B-allele frequency (BAF) profiles, tumor cellularity, and ploidy. Copy number/BAF profiles were all manually reviewed to generate comparable normalized profiles attributing copy number levels ranging from −2 (homozygous deletion), −1 (deletion), 0 (disomy), +1 (gain), +2 (gain of more than one copy), +3 (high level gains or amplification). Copy number frequency plots displaying the frequency of gains and losses across the cohort were generated genome-wide using these normalized values.

Heterogeneity

Phylogenetic trees were built based on a parsimonious, neighbor-joining method. In Figs. 2 and 3, trunks (blue in the Figures), clades (green) and branches (red) represented the alterations shared by all samples from one patient, alterations shared by at least two samples and private alterations, respectively. The heterogeneity ratio was calculated on the basis of Jaccard index between studied samples with the following formula:

$$HetR_{stud} = 1 - \frac{|A \cap B|}{|A \cup B|}$$

or

$$HetR_{stud} = 1 - \frac{\mathrm{NbAlt_{shared}}}{\mathrm{NbAlt_{shared}} + \mathrm{NbAlt_{sample1}} + \mathrm{NbAlt_{sample2}}}$$

where $\mathrm{HetR_{stud}}$ is the heterogeneity ratio of the studied sample pair, $\mathrm{NbAlt_{shared}}$ is the number of alterations shared by both samples, $\mathrm{NbAlt_{sample1}}$ is the number of alterations specific to sample 1, and $\mathrm{NbAlt_{sample2}}$ is the number of alterations specific to sample 1. HetR close to 0 thus corresponds to sample pairs sharing many mutations (homogeneous) while HetR close to 1 corresponds to sample pairs sharing very few mutations (heterogeneous).

Statistical analysis

Associations between qualitative and quantitative features were tested using Fisher exact test, Mann–Whitney *U* test, and Pearson test, respectively. Metastasis-free survival (MFS) was defined as the delay between the date of primary tumor treatment and the date of the first radiologic signs of histologically proven metastasis. MFS analysis was done using the Kaplan–Meier method and the Cox log-rank test. A two-tailed $P < 0.05$ was deemed statistically significant. Analyses were carried out with the R software version 3.4.2.

URLs

FastQC, http://www.bioinformatics.babraham.ac.uk/projects/fastqc/; Bowtie2 2.1.0, http://bowtie-bio.sourceforge.net/bowtie2/index.shtml; Picard Tool MarkDuplicates v1.97, https://broadinstitute.github.io/picard/; HaplotypeCaller, https://software.broadinstitute.org/gatk/documentation/tooldocs/current/org_broadinstitute_gatk_tools_walkers_haplotypecaller_HaplotypeCaller.php; MuTect2, https://software.broadinstitute.org/gatk/documentation/tooldocs/current/org_broadinstitute_gatk_tools_walkers_cancer_m2_MuTect2.php; SAMtools mpileup, http://samtools.sourceforge.net/; ANNOVAR, http://annovar.openbioinformatics.org/en/latest/; cosmic80, https://cancer.sanger.ac.uk/cosmic; Facets, https://github.com/mskcc/facets; maftools, https://bioconductor.org/packages/release/bioc/html/maftools.html; Pyclone, https://bitbucket.org/aroth85/pyclone/wiki/Home.

Data availability

Sequencing data have been deposited in and are available from the European Genome-phenome Archive database under number EGAS00001002761.

Results

Patient and tumor characteristics

We collected tumor samples from 25 patients eligible for therapeutic margin-free resection (R0 resection) of liver uveal melanoma metastases. Whole-exome sequencing (WES) from 25 germline DNA, 15 primary tumors (16 samples), and 47 metastases (75 samples) passed quality controls. We analyzed trios (germline, primary, metastases) in 15 cases. Median ages at primary uveal melanoma (PUM) and metastatic uveal melanoma (MUM) diagnoses were 55 (range 33–78) and 63 years old (range 33–80), respectively. Nine patients (9/25; 36%) were treated for their primary tumor with proton beam radiotherapy, two (8%) with brachytherapy, and 14 (56%) by enucleation, including one who received adjuvant photon radiotherapy. Adjuvant fotemustine was administered to one patient after inclusion in the FOTEADJ phase III clinical trial (ClinicalTrials.gov identifier: NCT02843386) (33). When metastatic, no systemic or local treatment was administered before metastases resection. Complete clinical and pathologic findings are described in Supplementary Table S1.

Mutation burden discriminates two classes of uveal melanoma, according to *MBD4* status

WES of tumor (primary and metastatic) and germline samples resulted in a median average depth of 158× and 70×, respectively (range 54–382× and 35–192×) and a median 20× coverage of 97% and 91%, respectively (range 81%–98% and 71%–97%). The vast majority of samples contained a low number of single nucleotide variants (SNVs; <23 SNVs per exome), while eight samples from two patients (#5 and #28) carried more than 250 SNVs (Fig. 1A). These hypermutated tumor samples were strikingly enriched in CpG>TpG transitions. Case #5 carried a *MBD4* deleterious germline mutation and somatic loss of the wild-type allele (12). Tumor samples from case #28 showed somatic deletion of *MBD4* and loss of the second chromosome 3 (Supplementary Fig. S1). Tumors from cases #5 and #28 were subsequently labeled as "MBD4def," for MBD4-deficient, while tumors from the 24 other cases, characterized by a low mutation burden and wild-type *MBD4*, were labeled as "MBD4pro" for MBD4-proficient. Given their contrasting mutation burdens, these uveal melanoma tumor types were analyzed separately.

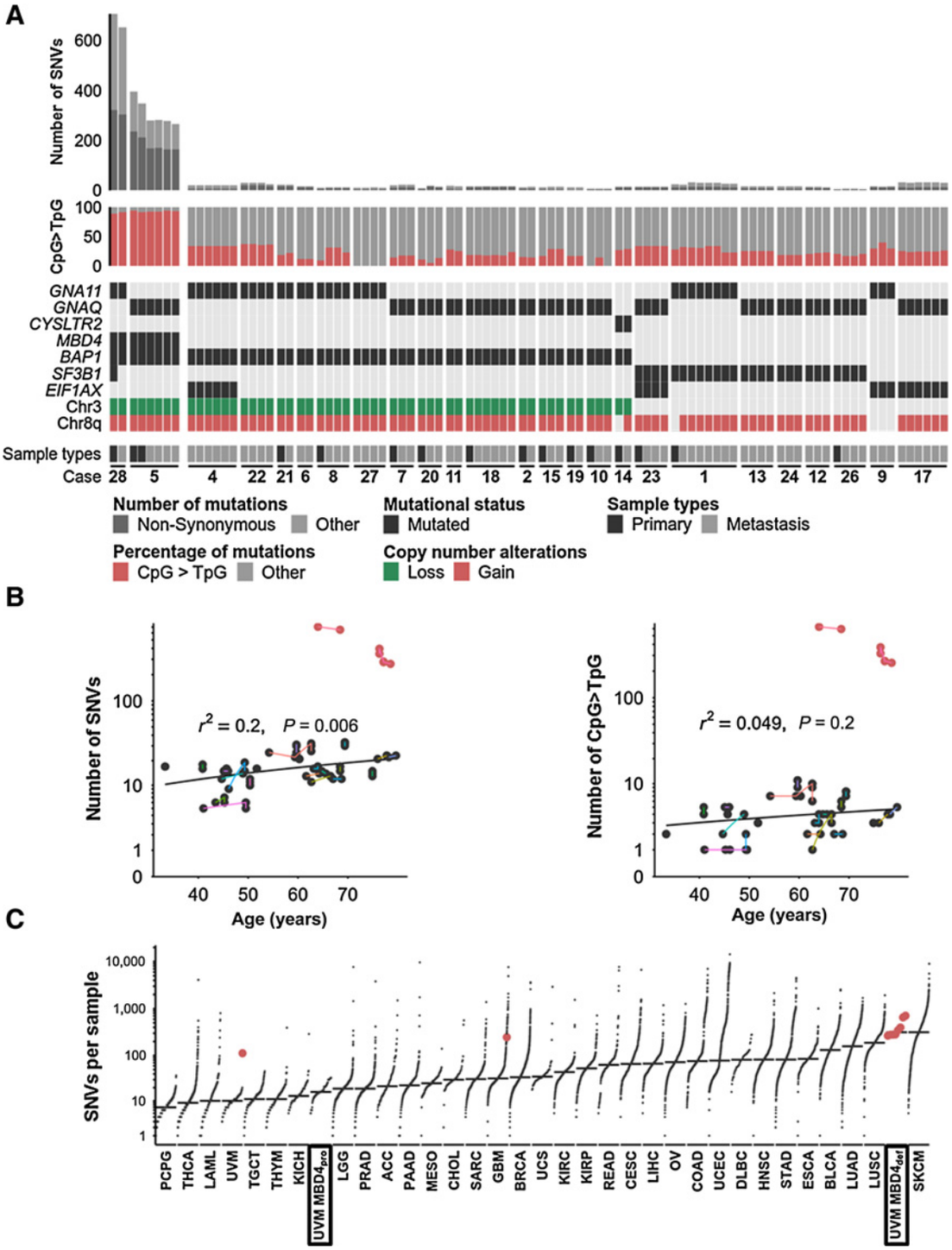

Figure 1.

Genetic characteristics and mutation burden. **A,** Genetic and clinical characteristics of sequenced samples. Panels from top to bottom: mutation burden (number of mutations per exome); proportion of CpG>TpG transitions; mutational status of *GNA11, GNAQ, CYSLTR2, MBD4, BAP1, SF3B1* and *EIF1AX*; status of chromosome 3 (loss; Chr3) and of chromosome 8 (gain of the long arm of chromosome 8; Chr8q) treatment; type of sample (primary or metastasis); and patient identifiers. **B,** Two-dimensional plots of mutation burden (left) and CpG>TpG transitions (right) in primary and metastatic uveal melanomas (*y*-axis) according to age at sampling (*x*-axis). Statistics were calculated considering only one single mean point for all tumors from a given patient at a given time. **C,** Mutation burden in MBD4pro and MBD4def UMs from our series compared with a pan-TCGA cohort. Samples from this series are framed. MBD4def tumors from this series and from TCGA are depicted by red dots.

We identified uveal melanoma–specific mutations in genes of the $G_{\alpha q}$ pathway (*GNAQ*, *GNA11* or *CYSLTR2*) and in *BAP1*, *SF3B1*, and *EIF1AX* (hereafter named "BSE") in all samples with high VAFs arguing for their early occurrence during the malignant process and subsequent clonal expansion (Fig. 1A). Mutations of the $G_{\alpha q}$ pathway were mutually exclusive in all cases. All samples with a *BAP1* deleterious mutation carried chromosome 3 loss of heterozygosity (LOH). BSE alterations were mutually exclusive in all but three cases: *EIF1AX*/*BAP1*-mutated, *EIF1AX*/*SF3B1*-mutated, and *BAP1*/*SF3B1*-mutated in cases #4, #23, and #28, respectively. High VAFs attested that both mutations coexisted in the same clones in cases #4, #23, but not in case #28. Similarly, mutational status of the $G_{\alpha q}$ pathway and BSE genes were identical in PUM and corresponding MUM, except for the MBD4def case #28, hereafter described in more detail. A small number of other candidate driver alterations was also found: a focal *CDKN2A* homozygous deletion in case #4; a hemizygous frameshift insertion of *CDKN2A* in case #17; *GNAS* R201C, hemizygous *TP53* R175H and *SMARCA4* T910M mutations in the MBD4def case #5. No driver mutation was recurrently acquired during metastatic progression.

MBD4pro PUM samples carried a median of 13 SNVs (range 5–25), similar to metastases that carried a median of 16 SNVs (range 5–33; Mann–Whitney $P = 0.17$), corresponding to a mutational rate over time (new SNVs between primary diagnosis and recurrence) estimated at 0.7 SNV per year. Few insertion/deletions (indel) were found (median = 1 per sample; range 0–5), primarily in the *BAP1* gene (10 cases). Mutation burden was significantly correlated with age, albeit with a low slope ($r^2 = 0.2$, log-rank $P = 0.006$; Fig. 1B), while number of CpG>TpG transitions were not significantly correlated with age ($r^2 = 0.049$, $P = 0.2$). No association was found between MUM mutation burden and histologic type, stage at diagnosis, adjuvant chemotherapy, or radiotherapy (all Mann–Whitney P values >0.05). Numbers of total SNVs and of CpG>TpG transitions between PUMs and paired MUMs were not correlated with time to metastatic recurrence (metastasis-free survival, MFS; $P = 0.3$ and 0.9, respectively; Supplementary Fig. S2).

In contrast, MBD4def PUM samples carried 348 to 706 SNVs per sample (>26-fold increase compared with MBD4pro) while metastases carried 266 to 652 SNVs (>16-fold increase). As expected, CpG>TpG median proportion among SNVs were significantly enriched in MBD4def samples as compared with MBD4pro (>89% vs. 24%, respectively; Mann–Whitney $P = 0.0009$).

Overall, MBD4pro PUMs and MUMs, the most frequent form of UMs, are associated with one of the lowest mutation burden observed in adult solid tumors, while MBD4def PUMs and MUMs carry a heavy mutation burden, in the same range as that observed in cutaneous melanomas (Fig. 1C; ref. 34).

Heterogeneity at the SNV level varies according to the *MBD4* status

We then compared the mutations (i) in primary tumors versus paired metastases (PUM/MUM comparison), (ii) in the different metastases from same patient (inter-MUM comparison), and (iii) in the different regions from the same metastasis (intra-MUM comparison). In MBD4pro cases, PUM/MUM inter-MUM and intra-MUM comparisons showed a median difference of 1.0 SNV [range, (−1.0–8.0)], 1.0 SNV (0.0–5.3), and 0.8 SNV (0.0–1.5), respectively. Low mutation burdens were associated with low heterogeneity ratios (HetR), which reflect the fraction of SNVs that are not shared between samples, in PUM/MUM, inter-MUM, and intra-MUM comparisons [median HetR of 0.11 (0.00–0.50), 0.17 (0.00–0.52), and 0.04 (0.00–0.19), respectively; Supplementary Fig. S3]. Altogether, these features correspond to simple evolutionary trees with a limited number of short clades and branches, including those from cases without primary tumors (Fig. 2A; Supplementary Fig. S4). Furthermore, quantitative analysis of VAFs with Pyclone (31), a method taking into account allelic imbalances and normal tissue contamination, also supported highly clonal and homogeneous structures of all MBD4pro uveal melanoma cases (Supplementary Fig. S5).

MBD4def tumors were much more heterogeneous than MBD4pro as PUM/MUM, inter-MUM, and intra-MUM comparisons showed high heterogeneity ratios (median HetR of 0.65, 0.53, and 0.18, respectively; Supplementary Fig. S3) resulting in longer clades and branches in evolutionary trees (Fig. 2A; Supplementary Fig. S4). MBD4def uveal melanoma presented a higher propensity to subclonality compared with MBD4pro. In case #5, the primary samples contained numerous subclones according to Pyclone analyses (Supplementary Fig. S5). In MBD4pro PUMs and MUMs, 12.4% of SNVs were different between PUM and corresponding MUM (i.e., private; 51 of 411 SNVs). Analysis of the cancer cell fraction (CCF) in PUMs and MUMs further attested to an exceedingly high level of homogeneity (Fig. 2B). In contrast, 98.3% of SNVs from MBD4def case #28 were private (1,201 of 1,222 SNVs). These SNVs appeared at the highest CCF levels in one sample while absent in the other (Fig. 2B). In case #5, CCF values from PUM samples were dispersed, reflecting a high heterogeneity in this sample, while metastases appeared more homogeneous (Fig. 2B; Supplementary Fig. S6), presumably due to a bottleneck effect during the metastatic process. Still, multiple sampling of metastasis #1 showed more than 20 private mutations in each region, which is probably the consequence of continuous acquisition of new SNVs after metastasis onset from a single clone. Altogether, MBD4 deficiency is associated with not only a high mutation burden but also a high heterogeneity in tumors at the SNV level, presumably because of the continuous mutagenic process.

Uveal melanomas show heterogeneity at the CNA level independent of *MBD4* status

At the copy number alterations (CNA) level, most samples presented simple CNA profiles consistent with diploid tumors containing few gains or losses of entire chromosomes or chromosome arms. In contrast, primary and metastatic samples from case #26 presented atypical profiles with numerous gains of entire chromosomes, while all samples from metastasis #1 of case #5 showed multiple gains and losses of entire chromosomes or chromosome arms in the context of *TP53* inactivation (Supplementary Fig. S1). Noticeably, case #17 showed evidence of chromothripsis on 8p. Different combinations of known uveal melanoma–typical CNA (i.e., losses of 1p, 3, 6q, 8p, gains of 1q, 6p, 8, 8q and isodisomy 3) were found in all samples. No `association was found between the number of CNA in MUM samples and histologic type, PUM stage, adjuvant chemotherapy, or adjuvant radiotherapy (all Mann–Whitney P values > 0.05).

In MBD4pro tumors, PUM/MUM comparison showed a median difference of 3.0 CNAs (0.0–6.0), while inter-MUM and intra-MUM comparisons showed a median difference of 1.0 CNA (0.0–8.0) and 0.0 CNA (0.0–7.3), respectively. Consequently,

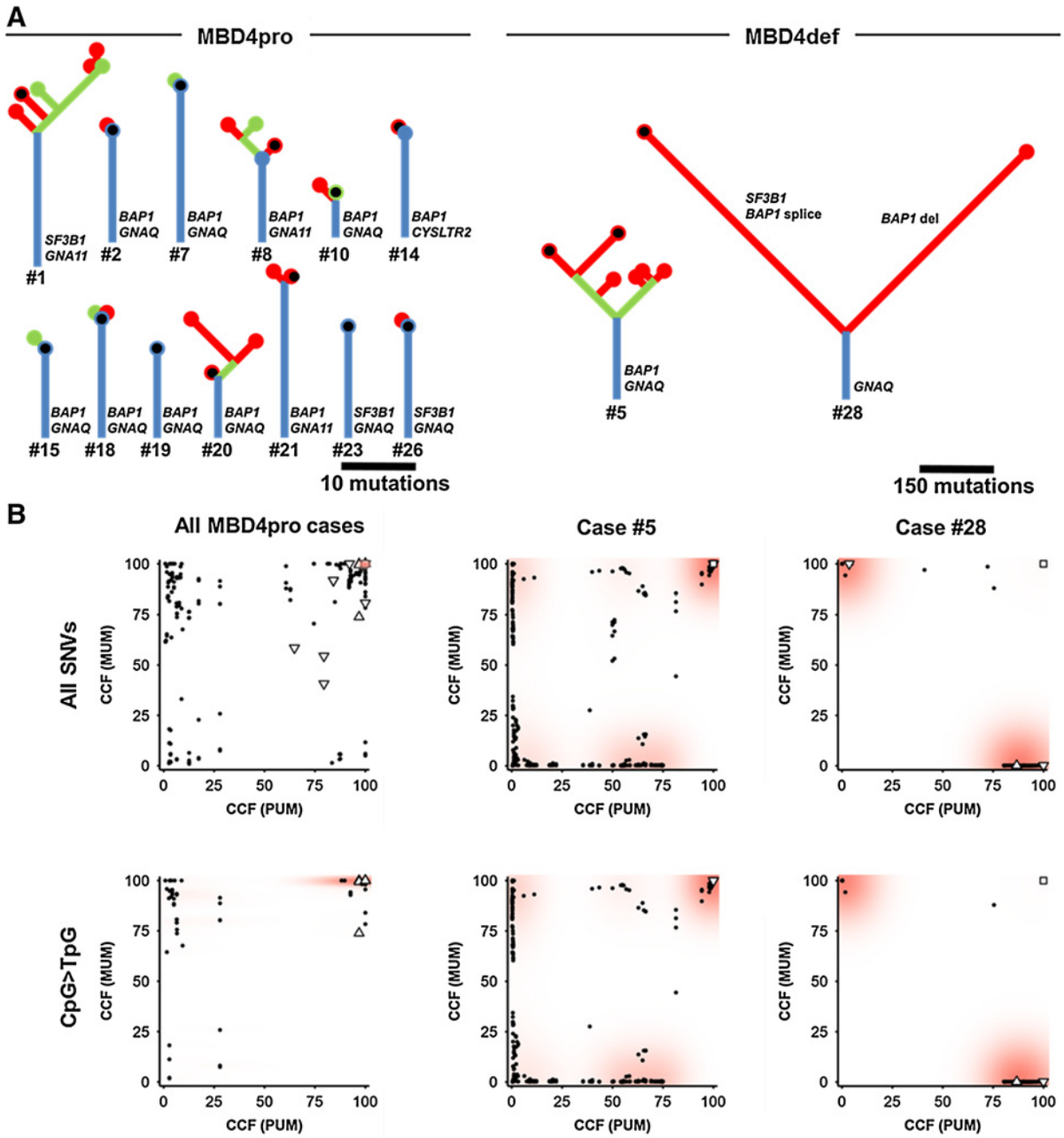

Figure 2.

Heterogeneity at the single nucleotide variant (SNV) level. **A,** Phylogenetic trees based on SNVs of the 13 MBD4pro (left) and 2 MBD4def (right) trios for which germline, primary tumor and metastases were sequenced. Primary tumors are marked with a black dot. Segments in blue represent the SNVs present in all samples, in green in at least two samples but not all, and in red in a single sample (private SNVs). Length of segments are proportional to number of SNVs according to the provided scale. **B,** Comparisons of CCFs between primary and metastatic samples. CCFs of all SNVs (top) and CpG>TpG only (bottom), in MBD4pro (left, pool of all MBD4pro samples) and MBD4def (right, each case analyzed independently) samples, are plotted with primary sample CCFs on the *x*-axis and metastatic sample CCFs on the *y*-axis. CCFs are corrected according to cell content, based on Gαq mutation CCF. Density of points is shown as a red gradient. In the "All SNVs/MBD4pro" plot, >75% of points are in the top right corner. Driver mutations are depicted by squares (*GNAQ, GNA11*, and *CYSLTR2*), triangles (*SF3B1*), inverse triangles (*BAPI*), and diamonds (*EIF1AX*).

HetR were high in PUM/MUM [median of 0.57 (0.00–0.92); Supplementary Fig. S3] compared with inter-MUM [median of 0.22 (0.00–0.83)] and intra-MUM comparisons [median of 0.00 (0.00–0.41)]. Although simple, CNA evolutionary trees revealed long clades and branches (Fig. 3A; Supplementary Fig. S4). Unequivocal intermediary levels of losses and gains were found in at least 10 samples out of 97, further supporting subclonality and copy number instability (Supplementary

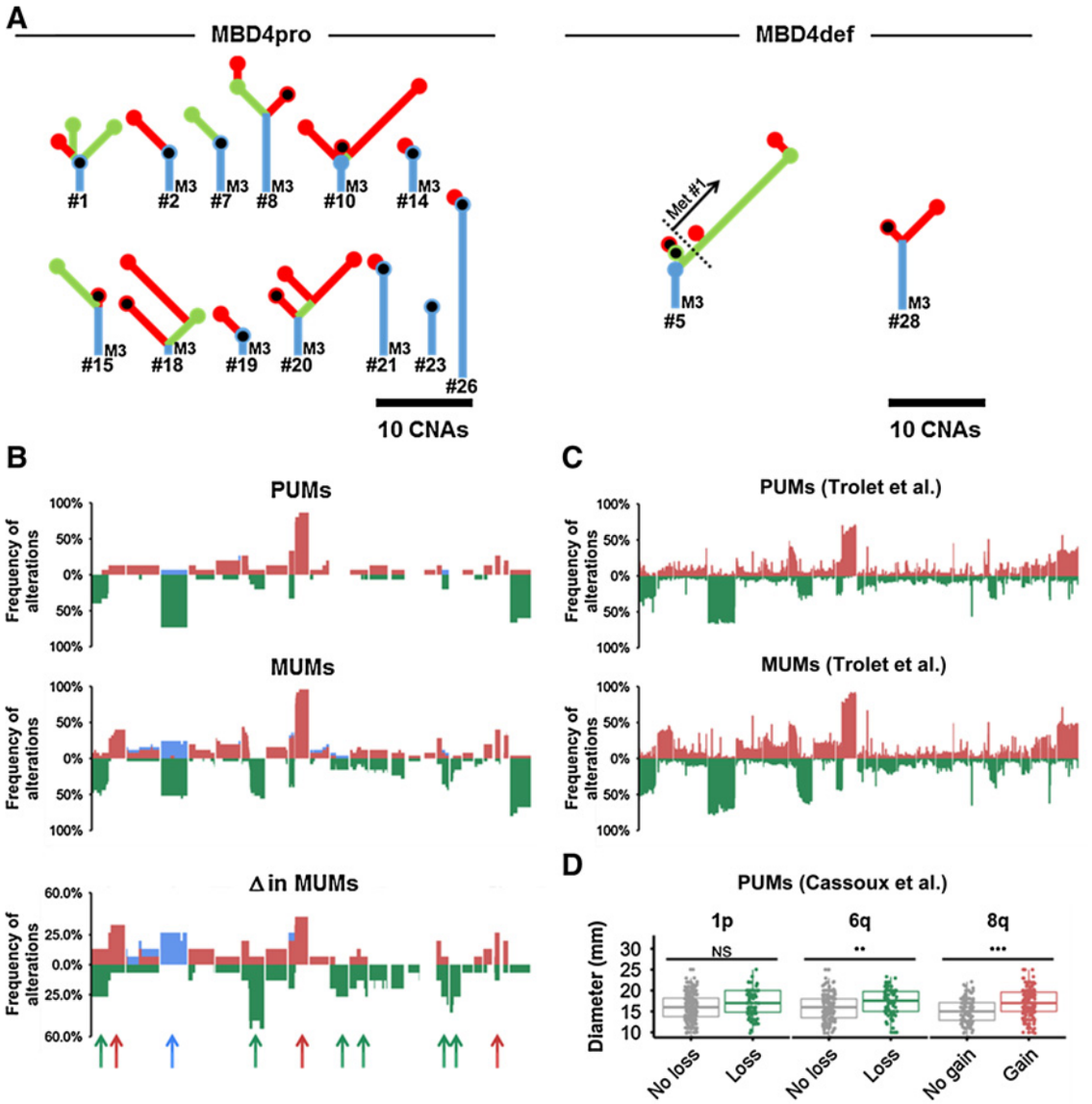

Figure 3.

Heterogeneity at the copy number alteration (CNA) level. **A,** Phylogenetic trees based on CNAs of the 13 MBD4pro (left) and 2 MBD4def (right) trios for which germline, primary tumor, and metastases were sequenced. Other phylogenetic trees from cases without primary tumors are presented in Supplementary Fig. S4. M3, monosomy 3. **B,** Global CNA profiles of this whole series of primary samples (top), metastatic samples (middle), and new CNAs appeared during metastatic progression (bottom). Chromosomes are distributed from chromosome 1 (left) to X (right). Gains, losses, and isodisomies are represented in red, green, and blue, respectively. *Y*-axis represents the frequency of the alteration in the series. Arrows highlight the most frequent alterations (at least 25% of cases). **C,** Global CNA profiles in an independent series of 86 PUMs and 66 unrelated MUMs (27). **D,** Diameter of primary tumors depending on the presence of 1p loss, 6q loss, or 8q gain in an independent series ($n = 321$; ref. 13). NS, Mann–Whitney $P > 0.05$; **, $P \leq 0.01$; ***, $P \leq 0.001$.

Fig. S1). MBD4def uveal melanoma copy number profiles were similar to MBD4pro, although HetR levels were substantially increased because of metastasis #1 from case #5 (Fig. 3A; Supplementary Fig. S3).

MUM contained a higher number of CNA than paired PUM (Fig. 3B; median = 10 vs. 5; Wilcoxon $P = 0.0038$). Five uveal melanoma–typical CNA (losses of 1p, 6q, gains of 1q, 8q, and isodisomy 3) and five atypical CNA (loss of 10p, 11qter, 16qter, 17pter, and gain of 21) were acquired during metastatic evolution in at least 4 cases. Of these, 6q loss was the most frequently acquired CNA (53%; 8/15 cases with primary profiles) and 8q gain was present in all but one metastases (96%; 24/25 cases). Noticeably, when 8q gain was already present in PUM, 8q levels were even higher in paired metastases in 23% of cases (3/13 cases with 8q gain). The increased frequency of these uveal melanoma–typical CNAs in MUMs, compared with unmatched PUMs, was confirmed in an independent series (isodisomy 3 could not be assessed for technical reasons; Fig. 3C; ref. 35). In contrast, the uveal melanoma–atypical CNAs were not recurrent in this independent series.

We then hypothesized that these CNAs may be a mark of tumor progression rather than of the metastatic process specifically. In an independent series of 338 PUMs, tumor size was indeed correlated with the presence of these uveal melanoma–typical CNAs, including a trend for 1p loss (median of 15.5 mm vs. 16.0 mm in 1p loss tumors; Mann–Whitney $P = 0.08$; Fig. 3D), a statistically significant association with 6q loss (15.0 mm vs. 17.0 mm; Mann–Whitney $P = 0.002$) and particularly 8q gain (14.4 mm vs. 17.0 mm; Mann–Whitney $P = 0.00001$). Association with 1q gain could not be tested because this variable had not been collected in this series (13).

Overall, these data showed that in contrast to the general stability observed at the nucleotide level, uveal melanomas acquire new uveal melanoma–typical CNA during tumor progression irrespectively of the *MBD4* status, tending toward a stereotyped profile when metastatic. However, loss of heterozygosity on chromosome 3, the main cytogenetic prognostic factor, was never acquired during tumor progression or in metastases.

Monosomy 3 defines earliness of relapse rather than the absolute risk of metastasis

Monosomy 3/*BAP1*-mutated uveal melanomas have been shown to be associated with a higher risk of metastasis than disomy 3, *SF3B1*, or *EIF1AX*-mutated uveal melanoma (8, 11, 13–15). We compared the incidence of prognostic genetic alterations in our series with two MUM and two PUM-independent series (11, 20, 36, 37). Incidences of BSE mutations were high and comparable across all MUM cohorts (Fig. 4A; *BAP1*: 65% vs. 56% and 56%, Fisher exact test $P \geq 0.57$; *SF3B1*: 26% vs. 29% and 26%, $P = 1$; *EIF1AX*: 17% vs. 7%, $P = 0.39$; *EIF1AX* status was not determined in one cohort; ref. 20). Unexpectedly, BSE mutations incidences in our MUM series were similar to what observed in two independent PUM series (*BAP1*: 65% vs. 43% and 48%, respectively; Fisher exact test $P \geq 0.10$; *SF3B1*: 26% vs. 22% and 21%, respectively; $P \geq 0.78$; *EIF1AX*: 17% vs. 12% and 17%, respectively; $P \geq 0.51$). Median MFS in patients with a monosomy 3 PUM from our series was significantly shorter than in other patients (Fig. 4B; 18.4 vs. 54.0 months, respectively; log-rank test $P = 0.007$). Because our series only included resectable metastases, we confirmed this difference of MFS in an independent series of unresectable MUM, in which patients with a monosomy 3 PUM also presented significantly shorter MFS (Fig. 4B; 38.1 vs. 83.2 months, respectively; log-rank test $P = 0.02$; ref. 37). Altogether, these results support that monosomy 3 and *BAP1* inactivation are not factors associated with a higher rate of metastatic recurrence but rather with a shorter time to metastasis.

MBD4 deficiency uncovers the timeline of genetic events

We showed that *MBD4* deficiency induces a high intratumor heterogeneity with numerous subclones, suggesting that this mutagenic process is probably continuous. We then took advantage of these features to explore more deeply MBD4def cases. In case #5, PUM sample #1 showed numerous clusters of subclonal SNVs (i.e., at intermediate levels of VAFs), which presumably developed during tumor progression. As an illustration, several potential driver alterations were present in the primary tumor including *SMARCA4* T910M, *GNAS* R201C, and *TP53* R175H (Fig. 5A). Analysis of sample #2 from the primary tumor demonstrated that these mutations occurred in different subclones, carrying the *SMARCA4* mutation without *GNAS*/*TP53* mutations (Fig. 5B). Further supporting this heterogeneity, metastases #1 and #2 carried different potential driver mutations (*GNAS*/*TP53* and *SMARCA4*, respectively) at high VAFs.

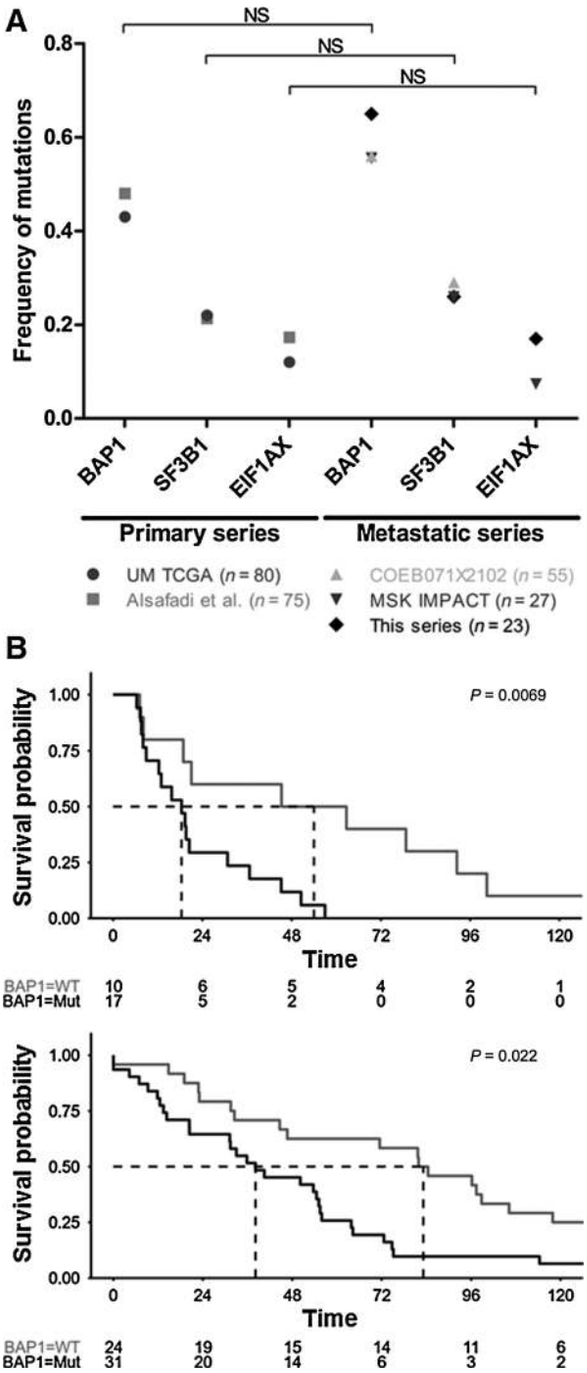

Figure 4.

Frequency of BSE alterations in five independent series and prognosis. **A,** Frequency of *BAP1, SF3B1*, and *EIF1AX* alterations in our series, two series of PUMs, and two series of unresectable MUMs (11, 20, 28, 29). NS, Fisher exact test $P > 0.05$. **B,** Kaplan–Meier metastasis-free survival curves in the current series (top) and in the NCT01430416 clinical trial (bottom).

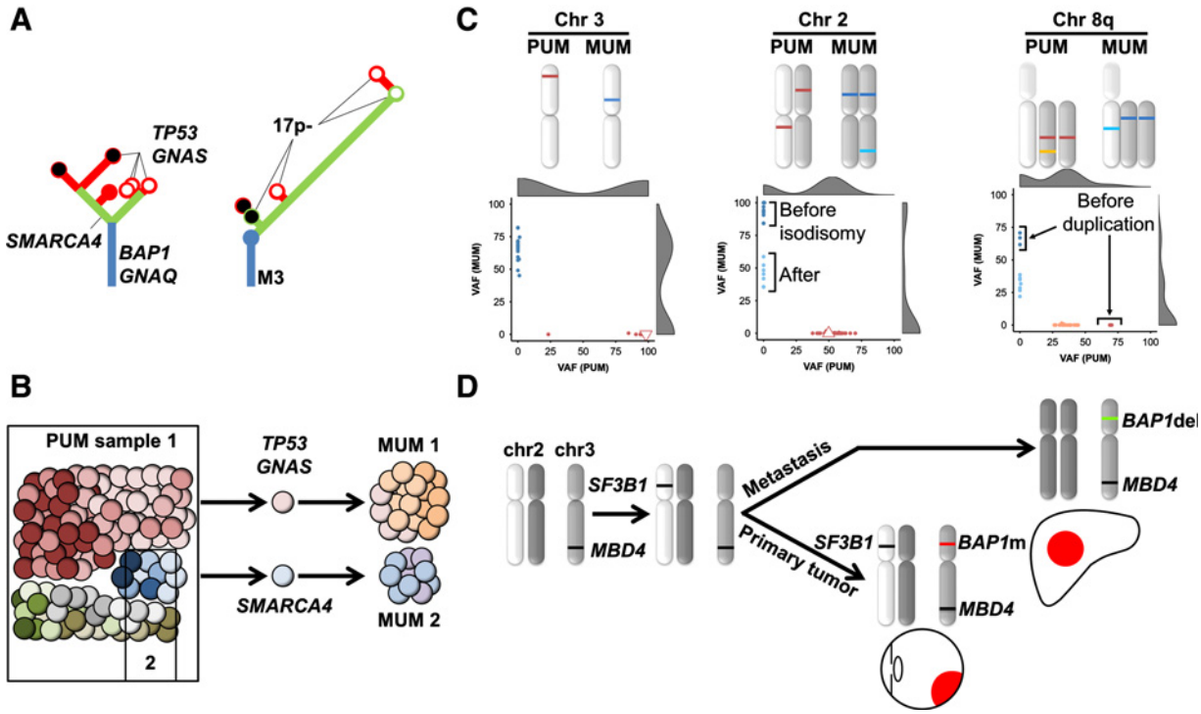

Figure 5.

MBD4 deficiency and timing of genetic events. **A,** Phylogenetic trees based on SNVs (left) and CNAs (right) in case #5. Samples from metastasis #1 and primary tumors are marked white and black dots, respectively. **B,** Schematic representation of the primary tumor and the two metastases from case #5. Colors represent the genetic background of the cells. Number of cells from each contingent is proportional to that observed. Red–orange cells are *TP53/GNAS*-mutated, blue–violet cells are *SMARCA4*-mutated, green–gray cells are not mutated in these genes. **C,** Independent evolution of the main primary and metastatic clones in case #28 illustrated by SNVs on chromosomes 2, 3, and 8. On top, schematic representations of chromosomal status. Light gray and dark gray indicate the two parental chromosomes. Colored bars illustrate examples of mutations in primary (orange and red) and in metastases (light and dark blue). Below, two-dimensional plots of SNVs according to VAF in the primary tumor (*X*-axis) and in the metastasis (*Y*-axis). On chromosome 2, dark blue dots and light blue dots represent mutations thought to have been acquired before and after isodisomy, respectively. On long arm of chromosome 8, dark blue and red dots represent mutations thought to have been acquired before duplication in metastatic and primary tumors, respectively. Light blue and orange dots represent mutations thought to have been acquired after duplication or on the other chromosome 8 in metastatic and primary tumors, respectively. **D,** Model of tumor progression in case #28 with monosomy 3 with focal chromosome 3 deletion encompassing *MBD4* as early event, followed by CpG>TpG *SF3B1* mutation. Then divergence between the main primary clone in the eye, characterized by the acquisition of a CpG>TpG, inactivating *BAP1* mutation, and the main clone in the liver metastasis with acquisition of a *BAP1* inactivating short indel, loss of the chromosome 2 carrying the *SF3B1* mutation, and duplication of the remaining chromosome 2.

Case #28 represented an extreme form of heterogeneity between PUM and MUM. First, the BSE status was not conserved between primary tumor and metastasis. While the primary tumor carried two pathogenic BSE mutations (*SF3B1* R625C and a *BAP1* intronic SNV that leads to aberrant splicing; Supplementary Fig. S7), the metastatic sample did not carry the *BAP1* intronic SNV but instead a *BAP1* frameshift indel, which was not detected in the primary tumor. The *SF3B1* mutation was absent from the metastasis, apparently by the loss of the chromosome 2 carrying the mutation, followed by the duplication of the remaining chromosome 2 (isodisomy 2). Furthermore, no SNV was shared between PUM and MUM chromosomes 2. Instead, chromosome 2 VAFs in the metastasis were distributed in two clusters: one with high values (~100% of cancer cells), likely to have occurred prior to chromosome 2 duplication and a second cluster at approximately 50% VAF or less, likely to have occurred after isodisomy (Fig. 5C). Globally, only 1.0% of CpG>TpG SNVs observed in tumor samples were shared between the primary tumor and the metastatic clone (12/1,195 at >5% of corrected VAF in both samples). Of these, no chromosome 3 SNV was shared between from PUM and MUM, arguing for the emergence of the mutator phenotype after loss of chromosome 3 and divergence of the two clones at this point. Similar analysis of chromosome 8 CpG>TpG VAFs showed that 8q duplication was an independent event in both samples, likely to have occurred after *MBD4* deficiency and thus after the loss of second chromosome 3. Altogether, these observations suggested the following relative order of genetic events in case #28: (i) the first events being the monosomy 3 and *MBD4* deletion, then (ii) *GNAQ* and *SF3B1* CpG>TpG driver mutations, (iii) followed by the emergence of the metastatic subclone, (iv) *BAP1* CpG>TpG mutation in the primary tumor, while the metastatic subclone acquired a *BAP1* indel mutation and lost one chromosome 2 with subsequent isodisomy 2 (Fig. 5D). These results argued for an early metastatic process in this case, soon after tumor onset and acquisition of monosomy 3 and *GNAQ*/*SF3B1* mutations, but before 8q duplication and *BAP1* mutations, with subsequent parallel evolution of lesions.

Discussion

Here we report the first extensive genetic analysis of metastatic uveal melanoma. We showed that, as for primary tumors,

MUMs carry one of the lowest mutation burdens across adult solid tumors (34). Therefore, the uveal melanoma metastatic process is not associated with a significant acquisition of genetic instability. Moreover, uveal melanoma driver alterations were conserved in metastases without new potential oncogenic mutations, supporting the idea that drivers are "set in stone," as recently hypothesized by Harbour and colleagues (3). In particular, we did not observe any switch from low-risk/disomy 3 genomic profiles in PUMs to high-risk/monosomy 3/*BAP1*-inactivated ones in metastasis. Furthermore, SNVs were present in high cancer cell fractions, attesting to the homogeneity of these tumors.

While uveal melanoma is a model of genetic stability and homogeneity at the SNV level, acquisition of new CNAs appears to be the main factor of genomic instability. Globally, CNA profiles evolved toward a stereotypical uveal melanoma profile, accumulating uveal melanoma–typical CNAs during the metastatic process as well as in the eye with the growth of the primary tumor. How these CNAs may contribute to tumor progression is not well understood. Gains of 6p have been associated with favorable prognosis in uveal melanoma, possibly because this region carries the HLA genes, but no correlation was observed between HLA expression and the number of 6p copies (38). No recurrent gene-inactivating mutations have yet been found associated with losses of 1p and 6q, suggesting a role for haploinsufficiency of these regions during tumor progression. Monosomy 3 was the only CNA that was never acquired during tumor progression. However, we found that isodisomy 3 was frequently associated with metastatic evolution of monosomy 3/*BAP1*-inactivated PUMs. Monosomy 3 is thought to foster tumor initiation through *BAP1* inactivation. Conversely, one can hypothesize that haploinsufficiency of chromosome 3 gene(s), such as *MITF*, *RHOA*, *RASSF1*, *MBD4* or *CTNNB1* (39), might reduce tumorigenic capacities, compensated by chromosome 3 duplication during tumor progression. Gain of 8q was more frequent in large primary tumors than in smaller ones and present in all but one metastatic samples, suggesting that this event is strongly associated with tumor progression. Further illustrating the importance of 8q gain in this disease, we showed that this CNA was acquired independently in the primary and the metastatic clones in one case, which attested to convergent evolution. The biological consequences of 8q gain are not yet understood, although the influence of several oncogenes such as *MYC* or *PTP4A3* has been suggested (40, 41).

The evolution of CNA profiles during tumor progression raised the question of uveal melanoma prognosis. Monosomy 3 and *BAP1* inactivation have previously been associated with poor prognosis (8, 13, 42). Strikingly, we observed the same distribution of high-risk/monosomy 3 profiles in MUM and PUM series. Our series presented a noticeable potential bias by the accrual of patients with resectable metastatic disease only, but we confirmed this finding in two independent series of patients with unresectable metastatic disease. Furthermore, we found that monosomy 3 and *BAP1* mutations were associated with a metastasis-free survival (MFS) more than twice as short as for disomy 3 tumors in two series, confirming recent results (43). Importantly, these results together with our analysis suggest that *BAP1* mutations and monosomy 3 are associated with the earlier occurrence of metastases, rather than with a higher absolute metastatic risk.

Our observations may have therapeutic implications as well. Although aggressive, MUMs are paradoxically highly resistant to all cytotoxic drugs. Tumor heterogeneity at the nucleotide level has been shown to contribute to drug resistance in some cancers, but it certainly does not explain chemoresistance in uveal melanoma. However, the contribution of tumor heterogeneity at the CNA or epigenetic levels for instance cannot be excluded. In contrast, stability at the nucleotide level hopefully forecasts that future targeted therapies against uveal melanoma might be associated with prolonged responses. Uveal melanomas are also frequently resistant to immune checkpoint inhibitors, potentially because of their low mutation burden. Conversely, high mutation burden due to *MBD4* deficiency has been shown to be associated

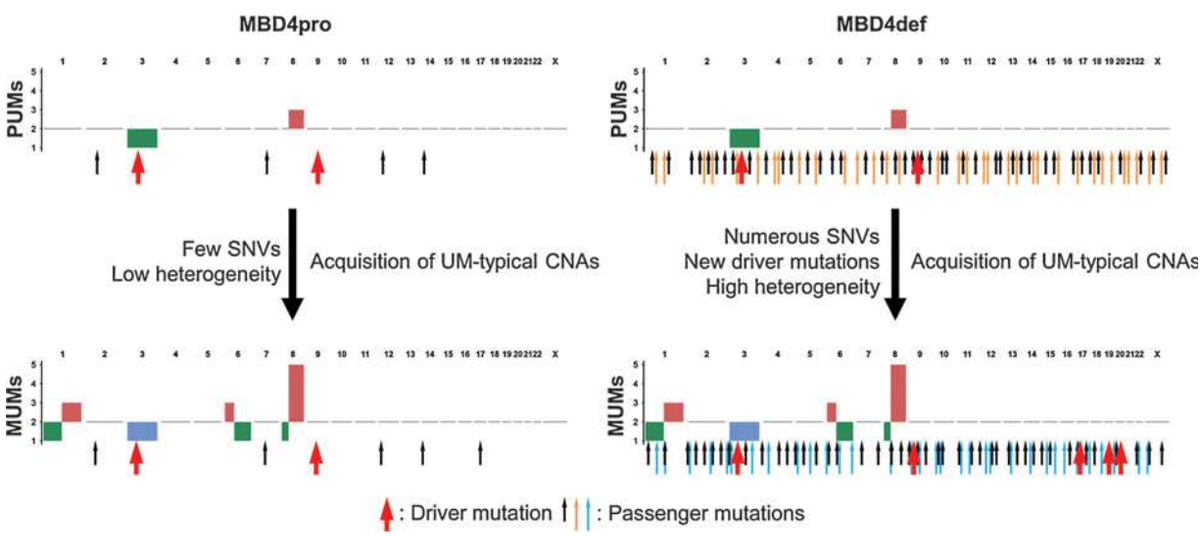

Figure 6.

Graphical summary of uveal melanoma genetic progression during the metastatic process, according to *MBD4* status. Chromosomes are distributed from chromosome 1 (left) to X (right) in each panel. CNAs are represented by colored rectangles with level of CNA on the *Y*-axis. Red arrows represent driver mutations; the other arrows are passenger somatic SNVs. Orange and blue arrows are SNVs that are private to the tumor, whereas black ones are shared between samples. UM, uveal melanoma.

with an outlier response to immune therapy (12, 44). However, McGranahan and colleagues showed that genetic heterogeneity was associated with resistance to immune therapies in lung cancer (45). Genetic heterogeneity in *MBD4*-deficient tumors may thus lead to secondary resistance, as occurred in the outlier response (12). Finally, analyses of MBD4def tumors revealed new CpG>TpG potential driver mutations such as *SMARCA4* T910M, *GNAS* R201C or *TP53* R175H. This hypermutated phenotype may thus lead to the discovery of new rare drivers (46, 47). Future work will reveal whether such mutations are associated specifically with uveal melanoma or rather with MBD4def across cancers, as we identified the same *SMARCA4* and *TP53* mutations in two *MBD4*-mutated tumors from TCGA cohorts, including a glioblastoma (11, 48). Altogether, MBD4def tumors appeared to be more mutated, more heterogeneous and more instable at the nucleotide level with the continual acquisition of oncogenic mutations than their MBD4pro counterparts while similar at the CNA level (Fig. 6).

Finally, we assessed the timing of the metastatic process. In MBD4pro cases, the small number of SNVs and high homogeneity of tumors prevented such analysis. However, the two MBD4def cases, with their high mutation burden and continuous acquisition of CpG>TpG transitions, were instrumental to circumvent these limitations. We showed that clones from MBD4def primary tumors and paired metastases shared as few as 1% of SNVs. Consequently, metastatic clones diverged from the primary tumor early after the first oncogenic events. In other words, if these mutations were acquired at a constant rate and if the tumor developed in, for example, five years, the metastatic clone would arise as soon as one month after the monosomy 3 event. Postulating that MBD4def and MBD4pro uveal melanomas share the same tumorigenic processes, we may predict that metastases occur early, long before diagnosis of the primary uveal melanoma. In the future, such a dismal hypothesis has to be tested in the more frequent, MBD4pro uveal melanoma cases. More generally, tumors with continuous genetic instability such as MBD4def tumors could be used as high-resolution genetic clocks to retrace tumor history.

Shain et al. (49) published a similar analysis on a comparable UM cohort and discovered *PBRM1* and other variants as potential driver mutations in UM metastases. We retrospectively analyzed our dataset and found a 19-bp deletion in the coding sequence of *PBRM1* (chr3:52610598-52610616) in a unique metastatic sample (metastasis #3 from case #10). Of note, we did not find mutations in *EZH2*, *PIK3R2*, *PIK3CA*, *PTEN*, or *MED12*, and no LOH on *GNAQ*, which were reported in Shain's series.

Disclosure of Potential Conflicts of Interest

E. Kapiteijn is a consultant/advisory board member for Roche, Novartis, Pierre-Fabre, Bristol-Myers Squibb, and Merck. No potential conflicts of interest were disclosed by the other authors.

Authors' Contributions

Conception and design: M. Rodrigues, L. Mobuchon, M.-H. Stern
Development of methodology: M. Rodrigues, S. Alsafadi, B. Marande, R.L. Barnhill
Acquisition of data (provided animals, acquired and managed patients, provided facilities, etc.): M. Rodrigues, S. Alsafadi, S. Baulande, O. Mariani, B. Marande, M.K. Van der Kooij, E. Kapiteijn, S. Gassama, R.L. Barnhill, V. Servois, S. Tick, N. Cassoux, G. Pierron, P. Mariani
Analysis and interpretation of data (e.g., statistical analysis, biostatistics, computational analysis): M. Rodrigues, L. Mobuchon, A. Houy, S. Alsafadi, K. Ait Rais, E. Kapiteijn, S. Gardrat, R.L. Barnhill, G. Pierron, J.J. Waterfall, M.-H. Stern
Writing, review, and/or revision of the manuscript: M. Rodrigues, L. Mobuchon, A. Houy, M.K. Van der Kooij, E. Kapiteijn, R.L. Barnhill, R. Dendale, S. Piperno-Neumann, G. Pierron, J.J. Waterfall, S. Roman-Roman, P. Mariani, M.-H. Stern
Administrative, technical, or material support (i.e., reporting or organizing data, constructing databases): M. Rodrigues, O. Mariani, M.K. Van der Kooij, N. Cassoux, G. Pierron
Study supervision: M. Rodrigues, M.-H. Stern
Other (pathologist): M. Putterman

Acknowledgments

This work was supported by funding from the European Commission under the Horizon 2020 program (UM Cure/to L. Mobuchon; project number: 667787), the INCa/ITMO/AVIESAN PhD fellowship program "Formation à la recherche translationelle" (to M. Rodrigues), the *Cancéropôle Ile de-France,* the INCa PRT-K14 UMCURE, the *Institut National de la Santé et de la Recherche Médicale* (INSERM), the Institut Curie, the *Ligue Nationale Contre le Cancer* (*Labellisation*), and the *Site de Recherche Intégrée sur le Cancer* (SiRIC) de l'Institut Curie. The Institut Curie ICGex NGS platform is funded by the EQUIPEX "*investissements d'avenir*" program (ANR-10-EQPX-03) and ANR10-INBS-09-08 from the *Agence Nationale de le Recherche*. The authors thank the patients and their family members. They also acknowledge support from the Institut Curie for sample collection, banking and processing: the Biological Resource Center and its members (O. Mariani), the Unité de Pharmacogénomique (Prof. I. Bièche) and the Histology Laboratory, Department of Pathology and its members (A. Vincent-Salomon); the Next Generation Sequencing team (V. Raynal, P. Legoix-Né); Novartis for sequencing data from the NCT01430416 clinical trial; Leanne de Koning and François-Clément Bidard for reviewing the manuscript.

The costs of publication of this article were defrayed in part by the payment of page charges. This article must therefore be hereby marked *advertisement* in accordance with 18 U.S.C. Section 1734 solely to indicate this fact.

Received April 11, 2019; revised May 29, 2019; accepted June 18, 2019; published first June 21, 2019.

References

1. Mahendraraj K, Lau CS, Lee I, Chamberlain RS. Trends in incidence, survival, and management of uveal melanoma: a population-based study of 7,516 patients from the Surveillance, Epidemiology, and End Results database (1973–2012). Clin Ophthalmol 2016;10:2113–9.
2. Furney SJ, Pedersen M, Gentien D, Dumont AG, Rapinat A, Desjardins L, et al. SF3B1 mutations are associated with alternative splicing in uveal melanoma. Cancer Discov 2013;3:1122–9.
3. Field MG, Durante MA, Anbunathan H, Cai LZ, Decatur CL, Bowcock AM, et al. Punctuated evolution of canonical genomic aberrations in uveal melanoma. Nat Commun 2018;9:116.
4. Moore AR, Ceraudo E, Sher JJ, Guan Y, Shoushtari AN, Chang MT, et al. Recurrent activating mutations of G-protein-coupled receptor CYSLTR2 in uveal melanoma. Nat Genet 2016;48:675–80.
5. Johansson P, Aoude LG, Wadt K, Glasson WJ, Warrier SK, Hewitt AW, et al. Deep sequencing of uveal melanoma identifies a recurrent mutation in PLCB4. Oncotarget 2016;7:4624–31.
6. Van Raamsdonk CD, Bezrookove V, Green G, Bauer J, Gaugler L, O'Brien JM, et al. Frequent somatic mutations of GNAQ in uveal melanoma and blue naevi. Nature 2009;457:599–602.
7. Van Raamsdonk CD, Griewank KG, Crosby MB, Garrido MC, Vemula S, Wiesner T, et al. Mutations in GNA11 in uveal melanoma. N Engl J Med 2010;363:2191–9.
8. Harbour JW, Onken MD, Roberson ED, Duan S, Cao L, Worley LA, et al. Frequent mutation of BAP1 in metastasizing uveal melanomas. Science 2010;330:1410–3.
9. Martin M, Masshofer L, Temming P, Rahmann S, Metz C, Bornfeld N, et al. Exome sequencing identifies recurrent somatic mutations in

EIF1AX and SF3B1 in uveal melanoma with disomy 3. Nat Genet 2013; 45:933–6.
10. Harbour JW, Roberson ED, Anbunathan H, Onken MD, Worley LA, Bowcock AM. Recurrent mutations at codon 625 of the splicing factor SF3B1 in uveal melanoma. Nat Genet 2013;45:133–5.
11. Robertson AG, Shih J, Yau C, Gibb EA, Oba J, Mungall KL, et al. Integrative analysis identifies four molecular and clinical subsets in uveal melanoma. Cancer Cell 2017;32:204–20.
12. Rodrigues M, Mobuchon L, Houy A, Fievet A, Gardrat S, Barnhill RL, et al. Outlier response to anti-PD1 in uveal melanoma reveals germline MBD4 mutations in hypermutated tumors. Nat Commun 2018;9:1866.
13. Cassoux N, Rodrigues MJ, Plancher C, Asselain B, Levy-Gabriel C, Lumbroso-Le Rouic L, et al. Genome-wide profiling is a clinically relevant and affordable prognostic test in posterior uveal melanoma. Br J Ophthalmol 2014;98:769–74.
14. Damato B, Dopierala JA, Coupland SE. Genotypic profiling of 452 choroidal melanomas with multiplex ligation-dependent probe amplification. Clin Cancer Res 2010;16:6083–92.
15. Onken MD, Worley LA, Tuscan MD, Harbour JW. An accurate, clinically feasible multi-gene expression assay for predicting metastasis in uveal melanoma. J Mol Diagn 2010;12:461–8.
16. Leyvraz S, Piperno-Neumann S, Suciu S, Baurain JF, Zdzienicki M, Testori A, et al. Hepatic intra-arterial versus intravenous fotemustine in patients with liver metastases from uveal melanoma (EORTC 18021): a multicentric randomized trial. Ann Oncol 2014;25:742–6.
17. Carvajal RD, Schwartz GK, Tezel T, Marr B, Francis JH, Nathan PD. Metastatic disease from uveal melanoma: treatment options and future prospects. Br J Ophthalmol 2017;101:38–44.
18. Mariani P, Piperno-Neumann S, Servois V, Berry MG, Dorval T, Plancher C, et al. Surgical management of liver metastases from uveal melanoma: 16 years' experience at the Institut Curie. Eur J Surg Oncol 2009;35:1192–7.
19. Robinson DR, Wu YM, Lonigro RJ, Vats P, Cobain E, Everett J, et al. Integrative clinical genomics of metastatic cancer. Nature 2017;548: 297–303.
20. Zehir A, Benayed R, Shah RH, Syed A, Middha S, Kim HR, et al. Mutational landscape of metastatic cancer revealed from prospective clinical sequencing of 10,000 patients. Nat Med 2017;23:703–13.
21. McGranahan N, Swanton C. Clonal heterogeneity and tumor evolution: past, present, and the future. Cell 2017;168:613–28.
22. Royer-Bertrand B, Torsello M, Rimoldi D, El Zaoui I, Cisarova K, Pescini-Gobert R, et al. Comprehensive genetic landscape of uveal melanoma by whole-genome sequencing. Am J Hum Genet 2016;99:1190–8.
23. Luscan A, Just PA, Briand A, Burin des Roziers C, Goussard P, Nitschke P, et al. Uveal melanoma hepatic metastases mutation spectrum analysis using targeted next-generation sequencing of 400 cancer genes. Br J Ophthalmol 2015;99:437–9.
24. Langmead B, Salzberg SL. Fast gapped-read alignment with Bowtie 2. Nat Methods 2012;9:357–9.
25. Lescai F, Marasco E, Bacchelli C, Stanier P, Mantovani V, Beales P. Identification and validation of loss of function variants in clinical contexts. Mol Genet Genomic Med 2014;2:58–63.
26. Cibulskis K, Lawrence MS, Carter SL, Sivachenko A, Jaffe D, Sougnez C, et al. Sensitive detection of somatic point mutations in impure and heterogeneous cancer samples. Nat Biotechnol 2013;31:213–9.
27. Li H, Handsaker B, Wysoker A, Fennell T, Ruan J, Homer N, et al. The Sequence Alignment/Map format and SAMtools. Bioinformatics 2009;25: 2078–9.
28. Wang K, Li M, Hakonarson H. ANNOVAR: functional annotation of genetic variants from high-throughput sequencing data. Nucleic Acids Res 2010; 38:e164.
29. Sherry ST, Ward M, Sirotkin K. dbSNP-database for single nucleotide polymorphisms and other classes of minor genetic variation. Genome Res 1999;9:677–9.
30. Forbes SA, Beare D, Gunasekaran P, Leung K, Bindal N, Boutselakis H, et al. COSMIC: exploring the world's knowledge of somatic mutations in human cancer. Nucleic Acids Res 2015;43(Database issue):D805–11.
31. Roth A, Khattra J, Yap D, Wan A, Laks E, Biele J, et al. PyClone: statistical inference of clonal population structure in cancer. Nat Methods 2014;11: 396–8.
32. Shen R, Seshan VE. FACETS: allele-specific copy number and clonal heterogeneity analysis tool for high-throughput DNA sequencing. Nucleic Acids Res 2016;44:e131.
33. Piperno-Neumann S, Rodrigues MJ, Servois V, Pierron G, Gastaud L, Negrier S, et al. A randomized multicenter phase 3 trial of adjuvant fotemustine versus surveillance in high risk uveal melanoma (UM) patients (FOTEADJ). J Clin Oncol 35:15s, 2017(suppl; abstr 9502).
34. Alexandrov LB, Nik-Zainal S, Wedge DC, Aparicio SA, Behjati S, Biankin AV, et al. Signatures of mutational processes in human cancer. Nature 2013;500:415–21.
35. Trolet J, Hupe P, Huon I, Lebigot I, Decraene C, Delattre O, et al. Genomic profiling and identification of high-risk uveal melanoma by array CGH analysis of primary tumors and liver metastases. Invest Ophthalmol Vis Sci 2009;50:2572–80.
36. Alsafadi S, Houy A, Battistella A, Popova T, Wassef M, Henry E, et al. Cancer-associated SF3B1 mutations affect alternative splicing by promoting alternative branchpoint usage. Nat Commun 2016;7:10615.
37. Piperno-Neumann S, Kapiteijn E, Larkin JMG, Carvajal RD, Luke JJ, Seifert H, et al. Phase I dose-escalation study of the protein kinase C (PKC) inhibitor AEB071 in patients with metastatic uveal melanoma. J Clin Oncol 32:15s, 2014(suppl; abstr 9030).
38. van Essen TH, van Pelt SI, Bronkhorst IH, Versluis M, Nemati F, Laurent C, et al. Upregulation of HLA expression in primary uveal melanoma by infiltrating leukocytes. PLoS One 2016;11:e0164292.
39. Sondka Z, Bamford S, Cole CG, Ward SA, Dunham I, Forbes SA. The COSMIC Cancer Gene Census: describing genetic dysfunction across all human cancers. Nat Rev Cancer 2018;18:696–705.
40. Laurent C, Valet F, Planque N, Silveri L, Maacha S, Anezo O, et al. High PTP4A3 phosphatase expression correlates with metastatic risk in uveal melanoma patients. Cancer Res 2011;71:666–74.
41. Parrella P, Caballero OL, Sidransky D, Merbs SL. Detection of c-myc amplification in uveal melanoma by fluorescent in situ hybridization. Invest Ophthalmol Vis Sci 2001;42:1679–84.
42. Prescher G, Bornfeld N, Hirche H, Horsthemke B, Jockel KH, Becher R. Prognostic implications of monosomy 3 in uveal melanoma. Lancet 1996; 347:1222–5.
43. Yavuzyigitoglu S, Koopmans AE, Verdijk RM, Vaarwater J, Eussen B, van Bodegom A, et al. Uveal melanomas with SF3B1 mutations: a distinct subclass associated with late-onset metastases. Ophthalmology 2016;123: 1118–28.
44. Johansson PA, Stark A, Palmer JM, Bigby K, Brooks K, Rolfe O, et al. Prolonged stable disease in a uveal melanoma patient with germline MBD4 nonsense mutation treated with pembrolizumab and ipilimumab. Immunogenetics 2019;71:433–6.
45. McGranahan N, Furness AJ, Rosenthal R, Ramskov S, Lyngaa R, Saini SK, et al. Clonal neoantigens elicit T cell immunoreactivity and sensitivity to immune checkpoint blockade. Science 2016;351:1463–9.
46. Johnson CP, Kim IK, Esmaeli B, Amin-Mansour A, Treacy DJ, Carter SL, et al. Systematic genomic and translational efficiency studies of uveal melanoma. PLoS One 2017;12:e0178189.
47. Piperno-Neumann S, Kapiteijn E, Larkin JMG, Carvajal RD, Luke JJ, Seifert H, et al. Landscape of genetic alterations in patients with metastatic uveal melanoma. J Clin Oncol 32:15s, 2014(suppl; abstr 9043).
48. Brennan CW, Verhaak RG, McKenna A, Campos B, Noushmehr H, Salama SR, et al. The somatic genomic landscape of glioblastoma. Cell 2013;155: 462–77.
49. Shain AH, Bagger MM, Yu R, Chang D, Liu S, Vemula S, et al. The genetic evolution of metastatic uveal melanoma. Nat Genet 2019;51:1123–30.